Proceedings of the 29th Annual International
Conference of the IEEE EMBS
Cité Internationale, Lyon, France
August 23-26, 2007.

Forehead Thermal Signature Extraction in Lie Detection

Zhen Zhu*, Panagiotis Tsiamyrtzis** and Ioannis Pavlidis*

Abstract— **Previous work demonstrated that facial thermography can be successful in lie detection. In those studies the development was based on the thermal signature of the periorbital region. In the present paper a new source of psychophysiological information is proposed: the forehead. We found that the corrugator muscle in the forehead is more active than usual, when the individual experiences sustained stress. As a result, more blood flows through the supraorbital vasculature, increasing the cutaneous forehead temperature. In order to monitor the thermal signature of the forehead's cutaneous tissue, a segmentation method based on active contours has been developed. This creates a virtual forehead probe that can monitor stress levels by measuring thermal radiation over the supraorbital vessels. Thermal videos of 38 subjects under interrogation for a mock crime scenario were used to test the new approach. The results show that the recovered forehead signal, enables 76.3% success rate in deceptive state classification. Thus, the forehead channel shows promise in lie detection.**

I. Introduction

Levine *et al.* reported in [1] a physiological signature on the periorbital region, directly associated with stress levels. One major application of this discovery is in lie detection [2]. In [3] Pavlidis *et al.* demonstrated that the new lie detection method produces comparable experimental results to traditional polygraphy. The added advantage is that the new method is contact-free and highly automated. Therefore, it can be applied on-the-fly in security checkpoint screening, as documented in [4].

In [5] Colin *et al.* reported that corrugator muscle activation is highly correlated with the existence of mental stress. This prompted us to investigate the applicability of the concept in lie detection. As in the case of the periorbital channel, activation of the muscle of interest is measured indirectly through the intensity of the thermal imprint of the supplying vessels. The vessels that supply with blood the corrugator muscle are the supraorbital vessels on the forehead. Whereas the periorbital signal carries information about instantaneous stress due to startle, the supraorbital signal carries information about longer lasting stress due to mental engagement. The hypothesis is that in the course of a screening interview, deceptive subjects may develop stronger mental engagement, as they are making up a story. From a practical perspective, the forehead Region of Interest (ROI) may serve as the main channel of information in cases where the periorbital ROI is off limits to thermal observation (e.g., the individual wears glasses).

*Zhen Zhu and Ioannis Pavlidis are with the Computational Physiology Lab, University of Houston, Houston 77204-30101, Texas, USA {zhu@cs.uh.edu ipavlidis@uh.edu}

**Panagiotis Tsiamyrtzis is with the Dept. of Statistics, Athens Univ. of Economics and Business, 76 Patission Street, 104 34 Athens, Greece pt@aueb.gr

A methodological problem that is still open is the segmentation of the thermal imprints of the supraorbital vessels. In [5] Colin *et al.* reported a heuristic segmentation method that certainly introduces non-trivial noise in the measurement process. A number of methods for segmenting blood vessels in various imaging modalities have been reported in the literature [6], [7], [8]. In thermal images, vessel imprints feature fuzzy edges due to thermal diffusion, which adds to the segmentation difficulty.

We propose a method based on Open-End Snake (OES) to segment the thermal imprints of the supraorbital vessels. Initialization of OES is aided by the operator. Thereafter, segmentation is carried out automatically, aided by the coalitional tracker [9]. We validate the segmentation goodness of the OES method using the overlapping ratio and Hausdorff distance. We test the lie detection potential of the forehead channel, based on OES vessel segmentation, by running predictions on the data set reported in [4]. For 38 subjects, the forehead deception classifier yields 76.3% success rate.

The remaining paper is organized as follows: In Section II, we present some background information on facial physiology and stress. In Section III, we describe the segmentation and tracking methods. In Section IV, we validate the segmentation method and compare it to other methods. We also provide the pattern recognition algorithm for deception detection and analyze the application level performance of OES. Finally, we conclude the paper in Section V.

II. Forehead Physiology and Stress

Every human being undergoes certain physiological changes under stress. The facial region is heavily innervated with neuronal pathways and it is not surprising that stress affects its physiology. Previous work has demonstrated that both the periorbital [1] and supraorbital [5] regions manifest stress signs.

One of the most salient manifestations of sustained stress is that the eyebrows frown more frequently [10]. The frowning is caused by the contraction of the corrugator muscle. Activation of the corrugator muscle requires more blood, which is drawn from the supraorbital vessels. The supraorbital vessels are found in the middle of the forehead and consist of two major branches and several sub-branches (see Fig. 1(a)). Increased blood flow in the supraorbital vessels, directly increases the cutaneous temperature on the forehead. In Fig. 1(b), the imprints of the supraorbital vessels are apparent within the rectangular annotation of the thermal image. Our task is to detect elevated stress levels through the quantification of increased vessel temperature in thermal imagery. The hypothesis is that this will provide a strong clue about the deceptive status of a subject, in a carefully designed and executed interview.

1-4244-0788-5/07/$20.00 ©2007 IEEE

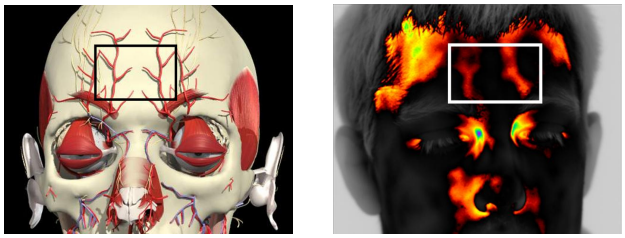

(a) Forehead Anatomy [11] (b) Thermal Facial Image

Fig. 1. Anatomical and thermal images of the face.

III. Forehead Signal Extraction

The thermal signal extraction proceeds in two steps. In step I, *segmentation* of the supraorbital vessels within the forehead ROI is taking place. In step II, the ROI and the segmented vessels therein are being *tracked* from frame to frame.

A. Step I: Segmentation

The proposed segmentation method features an open-end snake contour instead of a closed loop associated with the traditional model [12]. So, we call it Open End Snake (OES).

1) Open-End Snake: A traditional snake [12] is a curve $X(s) = [x(s), y(s)], s \in [0,1]$ that minimizes the energy functional

$$E = \int_0^1 \frac{1}{2}[\alpha|X'(s)|^2 + \beta|X''(s)|^2] + E_{ext}(X(s))ds. \quad (1)$$

The external energy E_{ext} is defined as the image intensity $E_{ext} = I(x,y)$. Thus, the snake contour has minimum energy when it matches the central line of the vessel. The curve equation $X(s)$ that minimizes Equation (1) must satisfy the Euler equation [7]:

$$\frac{\partial X(s,t)}{\partial t} = \alpha \frac{\partial^2 X(s)}{\partial s^2} - \beta \frac{\partial^4 X(s)}{\partial s^4} - \bigtriangledown E_{ext}. \quad (2)$$

When the solution of $X(s,t)$ approaches to a constant ($t \to \infty$), the left hand side of Equation (2) equals 0 and then the Euler equation has a valid solution.

2) Boundary and Initial Conditions: Both boundary conditions $X(s_0,t), X(s_n,t)$ and the initial condition $X(s,0)$ are required to solve Equation (2). In a traditional snake contour no boundary conditions are required. These are necessary though in our case, where the snake is employed as an open-end curve. Fortunately, these conditions can be achieved by refining the starting and ending points. The refinement procedure is illustrated in Fig. 2(a) and 2(b) and consists of the following steps:

1) Interpolate the initial points (A, M, and B) by a spline line. Evenly choose N interpolated points (x_1, x_2, …, x_{N-1}, x_N) on the spline line.
2) Refine the positions of two end points, at each end of the snake line. In Fig. 2(a), these correspond to points A and x_1 (at one end), x_N and B (at the other end). The refinement is accomplished by searching the maximum temperature locations along the normal lines that go across these four points (see Fig. 2(b)). After refinement, the four adjusted end points are A', x'_1, x'_N, and B' respectively.
3) The boundary conditions are given by these four new points, A', x'_1, x'_N, and B'. The initial condition is given by interpolating A', x'_1, M, x'_N, and B', as shown by the blue dotted line in Fig. 2(a).

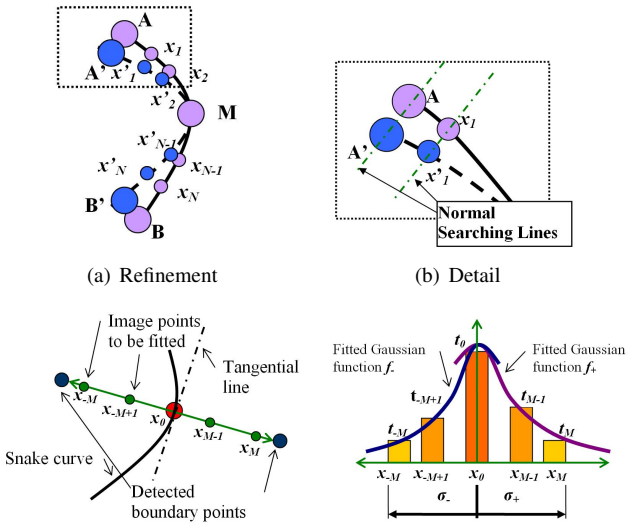

(a) Refinement (b) Detail

(c) Edge Detection (d) Temperature Profile

Fig. 2. Illustration of the OES algorithm.

Given that the tracking step is valid, the refinement steps automatically assure the correct boundary and initial conditions for OES.

3) Localization of Vessel Edges: By initializing the snake we located the vessel's central line. Next, we need to find the edges of the vessel. The basic idea is to fit temperature profiles of a Gaussian function along the vessel's radial direction. The detailed algorithm is as follows (refer to Fig. 2(c) and 2(d)):

1) Evenly select $N+1$ points from the snake curve $S_0, S_1, \ldots, S_N$. Then draw a normal line, perpendicular to the tangential direction of each of the $N+1$ points.
2) On each of the normal lines, choose $2M+1$ discrete temperature values $t_{-M}, t_{-M+1}, \ldots, t_0, \ldots, t_{M-1}, t_M$, corresponding to the locations x_{-M}, x_{-M+1}, …, $x_0, \ldots, x_{M-1}, x_M$ (see Fig. 2(c)).
3) Fit to these $2M+1$ temperature values two Gaussian functions: one, f_- fits the values from x_{-M} to x_0, while the other, f_+ fits the values from x_0 to x_{+M} (see Fig. 2(d)).
4) The width of the snake (i.e., vessel) at each point S_n is the sum of the standard deviations σ_- and σ_+ of the Gaussian functions f_- and f_+ (see Fig. 2(d)).
5) The final snake (vessel) boundary is obtained by connecting all $N+1$ boundary points at each side of the central line.

B. Step II: Tracking

We employ the coalitional tracker [9], which has been specially designed for tracking facial tissue. It can handle various head poses, partial occlusions, and inter-tissue region temperature variations. The tracking consists of the following steps:

1) The user selects a rectangular ROI on the initial frame. The selected ROI should cover the supraorbital vessels.
2) In the initial frame, the user also needs to select the initial location of the vessel. The selection consists of a series of points on the central line of the vessels.
3) The tracker estimates the best matching blocks in the next clip and then determines the initialization of each vessel in terms of the user selection. Next the segmentation step takes over the task of finding the exact vessel structure.

The tracking step is iteratively implemented until the end of the video sequence.

IV. Experimental Results

We have applied the forehead segmentation method on thermal clips from 38 subjects. These thermal videos were taken during interrogation, where a series of crime related questions were asked [4]. In this section we will compare the OES results with two other vessel segmentation methods. The first one is a morphological Tophat filter, which was used in segmenting generic facial vessels in infrared spectrum [8]. Comparison with Tophat will include segmentation goodness and application performance in lie detection. The second method is a heuristic algorithm that considers vessels are composed of the 10% hottest pixels in a carefully selected ROI. This method was used in periorbital vessel segmentation for lie detection [4]. It is not a true vessel segmentation method, but appears to capture the overall blood flow effect. Therefore, comparison with the 10% heuristic will be restricted on application performance.

A. Segmentation Performance

The segmentation ground truth for the experimental data set was created by manual delineation at a super-resolution level and based on our best anatomical knowledge.

Quantitative analysis of segmentation goodness was performed in terms of two measures: The overlap ratio and closeness. The overlap ratio is estimated by Accuracy [13], that is, the ratio of the correctly classified pixels. The higher the Accuracy is, the better the classifier. We calculated the Accuracy measure for the OES and the Tophat methods, over all 38 subjects. In Fig. 3(a), the results show that the mean Accuracy value over all 38 subjects is 95.8% for OES, and 80.9% for the Tophat, indicating that the new segmentation method is a lot more precise in detecting the supraorbital vessels on the forehead.

For further validation, we also used the Hausdorff distance [14], which measures the closeness of two vessels' contours. The lower the Hausdorff distance, the better the segmentation. The Hausdorff distances between the segmented vessels and

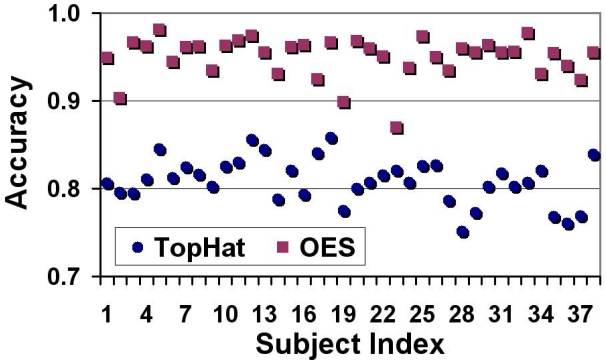

(a) The Accuracy measurement

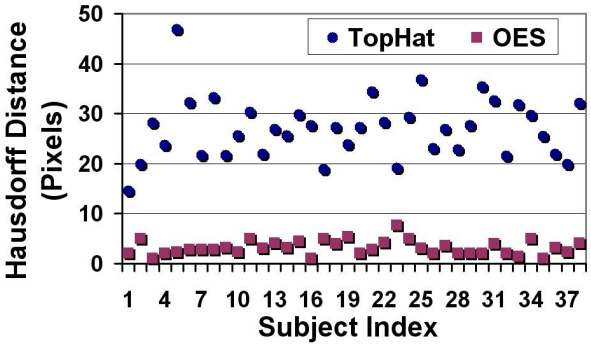

(b) The Hausdorff distance

Fig. 3. The comparison of validations for the OES and the morphological Tophat, over the 38 DARPA study subjects.

ground truth for the OES and Tophat methods are plotted in Fig. 3(b). We found that the OES method consistently outperforms the Tophat method, over all 38 subjects in the data set. The mean distance to the ground truth by using the Tophat is 26.97 pixels and it is only 3.69 pixels when the OES is used.

B. Performance Under Varying Conditions

We examined the robustness of the OES segmentation method as the head pose and forehead temperature varied. Fig. 4(a) shows a normal head pose for which the segmentation result is satisfactory. In Fig. 4(b) the subject looks upward. Still, the tracker locates correctly the forehead ROI and OES segments accurately the vessel, whose contour has become shorter. In Fig. 4(c), we observe that OES localizes the vessel contour even when the subject's forehead temperature has been raised. Fig. 4(d) shows the result of OES segmentation when the subject looks downward. It turns out that varying head poses and forehead temperatures do not cause any problems to the OES method. This hinges on the assumption that the ROI is not occluded in the video and the tracker performs well.

C. Performance on Lie Detection

In lie detection, we are interested in designing a pattern recognition scheme (classifier) that will be able to discriminate

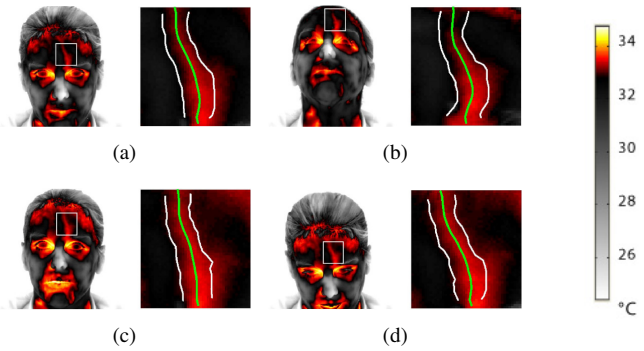

Fig. 4. Vessel tracking and segmentation results. The left image in each subfigure marks the ROI provided by the tracker and the right is the corresponding vessel detail.

the Deceptive (D) from the Non-Deceptive (ND) subjects. The classifier uses as raw data the supraorbital vessels' thermal signal, obtained by the OES segmentation. We found that the temperature variation, during an interrogation, is the result of the compounding effect of two phenomena: the interrogation effect (present to all subjects) and the deception effect (existing in D subjects only). Almost all of the subjects appear to have present the interrogation effect, since the forehead temperature appears to increase from the beginning to the end of the interrogation. For deceptive subjects, the deception effect is confounded with the interrogation effect. Our scheme aims to isolate the deception effect. We split the entire interview thermal signal to the 13 question-answer (Q&A) sessions. Please refer to [4] for the complete description of the relevant psychological experiment. For each of these sessions i we calculate the average temperature value of the thermal signal for the question part (Q_i) and the answer part (A_i), where $i = 1,2,\cdots,13$. Then, we calculate the difference for each session by $d_i = A_i - Q_i, i = 1,2,\cdots,13$. Next, we define:

$$\begin{aligned} D_I &= average(d_1,d_2), \\ D_{II} &= average(d_3,d_4,\cdots,d_{13}). \end{aligned}$$

Our decision rule is based on the comparison of D_I and D_{II}:

$$D_{II} - D_I \rightarrow \begin{cases} >0 & \text{Non-Deceptive}, \\ \leq 0 & \text{Deceptive} \end{cases} \quad (3)$$

This decision rule is based on the observation that deceptive subjects build stress sooner than non-deceptive subjects and they remain alert during the whole interview.

The final success rate of the proposed classifier is 76.3% for the OES segmentation method, 71.1% for the Tophat, and 68.4% for the 10% hottest heuristic segmentation. The prediction rate further motivates the use of the OES segmentation method. The detailed deception detection results are not displayed here due the limited space. Please refer to: http://www.cpl.uh.edu/html/localuser/zzhu/html/embs/Table_I.jpg

V. Conclusions and Discussion

We have developed a new segmentation method for extracting forehead signatures in thermal video clips that can be used in deception detection. It depends on tracking a forehead Region of Interest (ROI). Within the ROI, the supraorbital vessels are segmented using an Open-End Snake (OES). The experimental results show that the proposed method outperforms the Tophat and 10% hottest pixel methods in terms of segmentation goodness and/or application performance in lie detection.

There are a few problems concerning the new segmentation method. One is that the segmenter's performance depends heavily on the tracker's performance. One needs to find a more robust way to initialize the OES so that it can cope with occasional tracker instability. Another problem is the low performance of OES when the two supraorbital vessels are close to each other. Finally, the method cannot recover after temporary disappearance of the vessel's thermal imprint during the video.

Acknowledgment

This work was supported by a research contract from the Defense Academy for Credibility Assessment (DACA). Any opinions, findings, and conclusions or recommendations expressed in this material are those of the authors and do not necessarily reflect the views of the funding agency.

References

[1] J. Levine, I. Pavlidis, and M. Cooper, "The face of fear," *Lancet*, vol. 357, p. 1757, 2001.

[2] I. Pavlidis, N. Eberhardt, and J. Levine, "Seeing through the face of deception," *Nature*, vol. 415, p. 35, 2002.

[3] I. Pavlidis and J. Levine, "Thermal image analysis for polygraph testing," *IEEE Engineering in Medicine and Biology Magazine*, vol. 21, no. 6, pp. 56–64, November-December 2002.

[4] P. Tsiamyrtzis, J. Dowdall, D. Shastri, I. Pavlidis, M. Frank, and P. Ekman, "Imaging facial physiology for the detection of deceit," *International Journal of Computer Vision*, vol. 71, no. 2, pp. 197–214, October 2006.

[5] C. Puri, L. Olson, I. Pavlidis, J. Levine, and J.Starren, "Stresscam: non-contact measurement of users' emotional states through thermal imaging." in *Proceedings of the 2005 ACM Conference on Human Factors in Computing Systems*, Portland, Oregon, April 2-7 2005, pp. 1725–8.

[6] T. McInerney and D. Terzopoulos, "Deformable models in medical image analysis: a survey," *Medical Image Analysis*, vol. 1, no. 2, pp. 91–108, 1996.

[7] C. Xu and J. Prince, "Snakes,shapes, and gradient vector flow," *IEEE Transactions on Pattern Analysis and Machine Intelligence*, vol. 7, no. 3, pp. 359–69, March 1998.

[8] I. Pavlidis, P. Tsiamyrtzis, C. Manohar, and P. Buddharaju, *Biometrics: face recognition in thermal infrared*, 3rd ed., ser. Biomedical Engineering Handbook. CRC Press, 2006, ch. 29, pp. 1–15.

[9] J. Dowdall, I. Pavlidis, and P. Tsiamyrtzis, "Coalitional tracking," *Computer Vision and Image Understanding*, vol. 106, no. 2-3, pp. 205–219, May-June 2007.

[10] P. Ekman, W. Friesen, and J. Hager, *THE FACIAL ACTION CODING SYSTEM*, 2nd ed. London: Weidenfeld & Nicolson (world), 2002.

[11] B. J. Moxham, C. Kirsh, B. Berkovitz, G. Alusi, and T. Cheeseman, "Interactive head & neck (CD-ROM)," Primal Pictures, December 2002.

[12] M. Kass, A. Witkin, and D. Terzopoulos, "Snakes: active contour models," *International Journal of Computer Vision*, vol. 1, no. 4, pp. 321–331, 1987.

[13] R. Kohavi and F. Provost, "Glossary of terms," *Machine Learning*, vol. 30, pp. 271–274, 1998.

[14] D. Huttenlocher, D. Klanderman, and A. Rucklige, "Comparing images using the Hausdorff distance," *IEEE Transactions on Pattern Analysis and Machine Intelligence*, vol. 15, no. 9, pp. 850–863, September 1993.